# In-Situ Mass-to-Charge Ratio Measurement and Trajectory Control of a Vertically Injected Laser Fusion Energy Charged Target via Electric Field

Ryusuke TSUJI

*Department of Electrical and Electronic Systems Engineering, Ibaraki University, Hitachi 316-8511, Japan*

(Received 26 September 2020 / Accepted 17 April 2022)

A method is presented for controlling the trajectory of a vertically injected charged spherical laser fusion target. The position and time of the injected target in flight are measured in a position measurement unit using the Arago spot. After the target passes between the first pair of deflection plates, where there exists a constant electric field, the mass-to-charge ratio of the target in flight is obtained from the shift in its trajectory. The amplitude of the electric field applied between the second and third pairs of deflection plates is calculated using this ratio. After passing through the second and third pairs of deflection plates, the target deflects its trajectory to pass through the reactor center. The design parameters of the trajectory control system for a tabletop plasma device and a laser fusion reactor are presented.



Keywords: trajectory control, laser fusion energy target, position measurement unit, Arago spot, mass-to-charge ratio

DOI: 10.1585/pfr.17.1404088

## 1. Introduction

In direct-drive laser fusion, a spherical fuel target is injected into the reactor chamber, where laser fusion occurs. The position and time of the injected target in flight are measured. However, the trajectory must be calculated within a few milliseconds to predict the arrival position and time of the target at the reactor center. The focal points of hundreds of laser beams must be moved to the arrival position. The engagement error in the laser beam and the target at the main implosion shot must be lower than 20 μm [1].

To avoid or reduce the difficulty in controlling hundreds of final optical components, several methods to control the target trajectory have been proposed instead of controlling the final optical component, e.g., the magnetic control method [2,3] and the electrostatic control method [4,5]. The above methods adjust the trajectory of the target to pass through the reactor center onto which hundreds of laser beams are focused.

In the magnetic control method, the spherical target is coated with a Pb layer and cooled below 7.2 K. The target is injected through symmetrically placed magnets. The cooled target becomes superconducting state and is subjected to the repulsion force from the magnets. The target deflects its trajectory and hits the reactor center. To cool Pb from 17 K down to 7.2 K, a low vibration system and a thermal shield are required as the specific heat of Pb at 7 K is around one order of magnitude less than that at 17 K [6].

The electrostatic control method uses an electric field to achieve the continuous dynamic control of the trajectory of a charged target. The direct-drive spherical target is coated with a very thin metal layer to reflect the radiation from the hot chamber wall [7]. The spherical target is considered as a spherical conductor. The target is in touch with the high-voltage injector and is launched. In the pioneering study of Petzoldt *et al*., the target was charged, and an electric field was applied to adjust the trajectory of the target [4, 5]. The authors used a parallel laser beam to continuously illuminate the freely falling target. The two-dimensional (2D) Arago (Poisson) spot image was processed every 8 ms to measure the $x$- and $y$-coordinates of the charged target [4]. However, in the case of a 100-m/s injection, the processing time of the 2D Arago spot image is too long. Parallel laser illumination to the target reduces the spatial resolution to measure the target position at a large distance. In addition, continuous illumination reduces the time resolution. Thus, numerous improvements can still be made to the existing setup. Precise measurements of the position and time of the charged target enable the precise control of the target trajectory using an electric field.

In this study, a simple and precise control method of the target trajectory is proposed using an electric field. Orthogonal pulsed divergent laser illumination is used on the flying charged target to measure precisely its position and time [8]. The mass-to-charge ratio of the target in flight is first measured. Although the charging voltage at the target release is constant, the charge on the target changes at every injection [4]. Furthermore, it is difficult to measure the mass and charge of the target in flight. However, the

*author's e-mail: ryusuke.tsuji.prof@vc.ibaraki.ac.jp*

precise measurement of the position and time of the flying target in an electric field provides a precise mass-to-charge ratio without knowing neither the mass nor the charge of the target. This ratio is the most important parameter in the calculation of the target trajectory in an electric field. After determining this ratio, the magnitude of the electric field required to force the target to pass through the reactor center can be calculated. This control electric field is applied between the deflection plates before the target passes through them. The target adjusts its path accordingly and hits the reactor center.

The trajectory control system is presented in Sec. 2, and the measurement method for the mass-to-charge ratio is described in Sec. 3. The procedure to calculate the magnitude of the control electric field required to adjust the trajectory is presented in Sec. 4. Recently, a vertical target injection and engagement system were built and operated at 1 Hz [9–12]. The design parameters of the trajectory control system for two potential applications, namely a high-repetition plasma generation device and a laser fusion reactor, are provided in Sec. 5. Finally, the conclusions are drawn in Sec. 6.

## 2. Trajectory Control System

The trajectory control system is illustrated in Fig. 1. The charged spherical target flies in vacuum from the top and enters the reactor chamber when the shutter opens.

The *XYZ*-coordinate system is introduced both in the global coordinate system and in the local coordinate system in the position measurement unit (PMU). The origin of the global coordinate system is set to be the reactor center, i.e., the fixed focus of the implosion laser. The origin of the local *XYZ*-coordinate system is marked with a cross at the center of each $\mathrm{PMU_i}$ (i = 1, 2, 3) and corresponds to (0, 0, $H_\mathrm{i}$) in the global *XYZ*-coordinate system. In our previous study [13], the placement error in the PMU was experimentally evaluated through one test injection. After calibrating the placement error, the local coordinates and time of the injected target in the PMU can be transformed into global coordinates, i.e., the measured local coordinates of the target ($dx_\mathrm{i}$, $dy_\mathrm{i}$, $dz_\mathrm{i}$, $T_\mathrm{i}$) in the $\mathrm{PMU_i}$ are converted into global coordinates ($dx_\mathrm{i}$, $dy_\mathrm{i}$, $H_\mathrm{i} + dz_\mathrm{i}$, $T_\mathrm{i}$). A first pair of parallel electrodes (A) is set between the $\mathrm{PMU_2}$ and the $\mathrm{PMU_3}$ to measure the mass-to-charge ratio. A second pair of parallel electrodes (B) is placed between the $\mathrm{PMU_3}$ and the chamber wall to generate a constant electric field $E_x$, which deflects the trajectory of the injected charged target. A third pair of parallel electrodes (C) is used to generate a constant electric field $E_y$, which also deflects the target trajectory.

In this study, the distance $d$ between the deflection plates is assumed to be ~0.02 m, i.e., much smaller than the plate length $L$ ($d \ll L$). Thus, for simplicity of discussion, the electric field is assumed to exist only between the deflection plates. The spherical charged target is treated as a point charge. The acceleration and deceleration of the charged target in the fringe field of the plate are neglected.

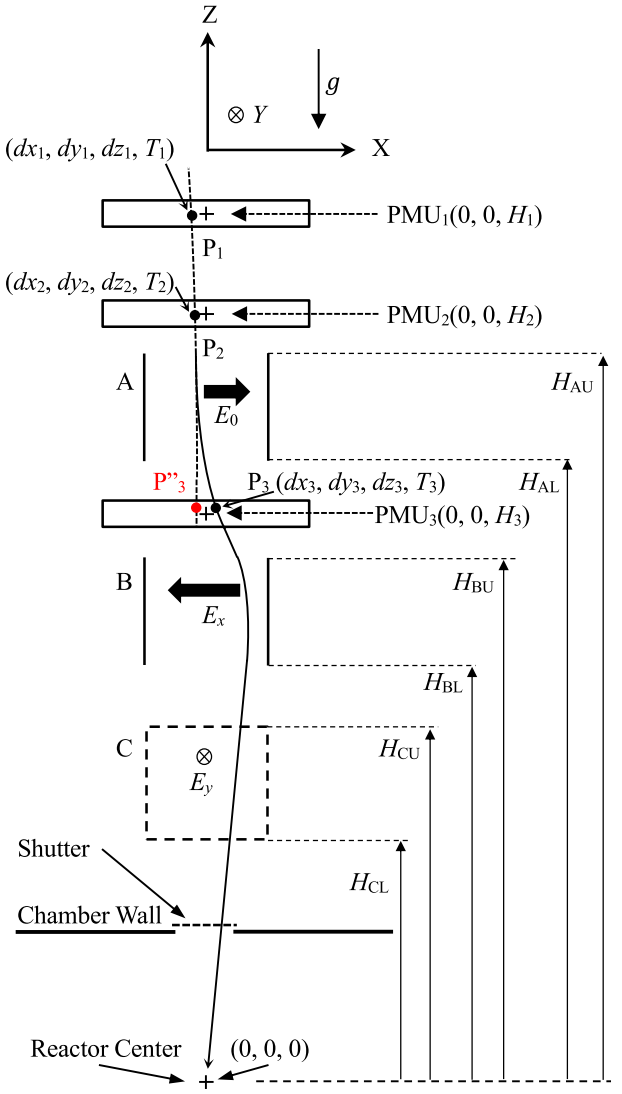


Fig. 1 Trajectory control system. The pairs of electrodes A and B are parallel to the *YZ*-plane. The pair of electrodes C is parallel to the *XZ*-plane. $H_\mathrm{AU}$, $H_\mathrm{BU}$, and $H_\mathrm{CU}$ are the upper heights of the electrodes A, B, and C, respectively, whereas $H_\mathrm{AL}$, $H_\mathrm{BL}$, and $H_\mathrm{CL}$ are the corresponding lower heights.

The charged target is injected from the top. When the target is detected in the $\mathrm{PMU_i}$ (solid box) in Fig. 1, it is automatically irradiated by orthogonal pulsed laser beams at the points $\mathrm{P_1}$, $\mathrm{P_2}$, and $\mathrm{P_3}$ at times $T_1$, $T_2$, and $T_3$, respectively, as represented by the black points in Fig. 1. The timings of the laser illumination for the target position measurement in each PMU are shown in Fig. 2.

The target crosses two parallel Rays, namely $\mathrm{Ray_1}$ and $\mathrm{Ray_2}$, and the times at which the voltage of the photodiode decreases, namely $T_\mathrm{Ray1}$ and $T_\mathrm{Ray2}$, are detected [9, 11, 12]. The distance between $\mathrm{Ray_1}$ and $\mathrm{Ray_2}$ is $\Delta L \approx 0.01$ m. As a time difference is $\Delta T = T_\mathrm{Ray2} - T_\mathrm{Ray1}$, the target is then located a distance $\Delta L$ below $\mathrm{Ray_2}$, which corresponds to

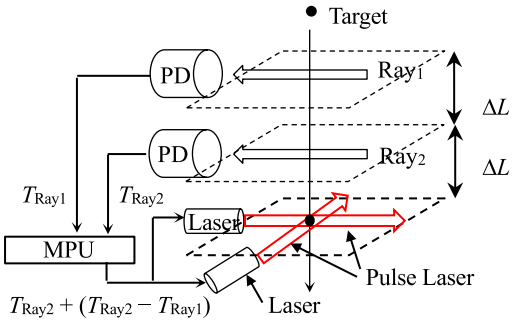


Fig. 2 Schematic of the interior of the PMU. PD denotes the photodiode. The target crosses $\mathrm{Ray}_1$ and $\mathrm{Ray}_2$ at times $T_{\mathrm{Ray1}}$ and $T_{\mathrm{Ray2}}$, respectively. $\Delta L$ is the distance between $\mathrm{Ray}_1$ and $\mathrm{Ray}_2$.

Table 1 Local and global coordinates.

| Point | Local coordinate | Global coordinate |
|---|---|---|
| $P_1$ | $(dx_1, dy_1, dz_1)$ | $(dx_1, dy_1, H_1+dz_1)$ |
| $P_2$ | $(dx_2, dy_2, dz_2)$ | $(dx_2, dy_2, H_2+dz_2)$ |
| $P_3$ | $(dx_3, dy_3, dz_3)$ | $(dx_3, dy_3, H_3+dz_3)$ |
| $P"_3$ | $(dx"_3, dy_3, dz_3)$ | $(dx"_3, dy_3, H_3+dz_3)$ |

the position measurement region at $T_{\mathrm{Ray2}} + \Delta T$. The target is irradiated by orthogonal pulsed laser beams.

The precise target position in the PMU is obtained using the Arago spot method. The Arago spot is a tiny bright spot that appears at the central portion of the geometrical shadow of the spherical target. A divergent beam illumination magnifies the shadow, enabling remote measurements without reducing the spatial resolution [8]. The target with a velocity of 100 m/s moves by 1 μm in 10 ns. Irradiating the spherical target with an orthogonal pulsed laser with a duration of less than 10 ns permits the measurement of the position and time of the injected target with an accuracy of less than 1 μm for a 100-m/s injection. Image compression using a cylindrical lens can convert the 2D Arago spot image into a one-dimensional image [14]. This technique reduces the amount of data and enables real-time data processing for trajectory control.

The time variable can be considered as a global variable by supplying common clock pulses to each PMU. The local and global coordinates of the points are presented in Table 1.

The target deflects its trajectory due to the $E_0$ electric field between the A plates and reaches the point $P_3$ at time $T_3$. The point $P"_3$ represented in red in Fig. 1 is the calculated target position at time $T_3$ in the case of no applied electric field. The mass-to-charge ratio of the target can be derived from the difference between the coordinates of the points $P_3$ and $P"_3$. After passing through the second and third pairs of deflection plates, the target passes through a temporally opened shutter and moves along the trajectory that passes through the reactor center (0, 0, 0). The time sequence of the target motion is illustrated in Fig. 3.

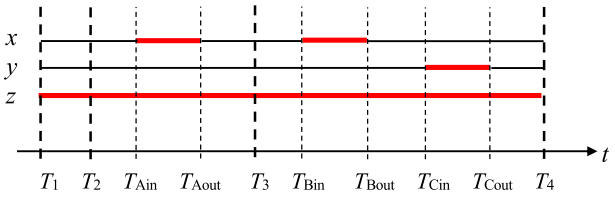


Fig. 3 Time sequence of the target motion. The thick red segments represent accelerated motion, whereas the thin black segments represent motion with a constant velocity.

## 3. Measurement of the Mass-to-Charge Ratio

The position and velocity of the injected target in the $\mathrm{PMU}_1$ are assumed to be $(dx_1, dy_1, H_1 + dz_1)$ and $(v_{x1}, v_{y1}, v_{z1})$ at $T_1 = 0$, respectively. These values are used to determine the mass-to-charge ratio. The local position $(dx_1, dy_1, dz_1)$ is measured by the $\mathrm{PMU}_1$. The velocity of the target at $T_1 = 0$ is obtained from the $\mathrm{PMU}_1$ and $\mathrm{PMU}_2$ data as follows.

The equation of motion for the $x$-direction is described as:

$$m\frac{dv_x}{dt} = 0, \tag{1}$$

where $m$ is the mass of the target. The $x$-component of the velocity and the position of the target are:

$$v_x(t) = v_{x1}, \tag{2}$$

$$x(t) = v_{x1}t + dx_1, \tag{3}$$

where $v_{x1}$ is the $x$-component of the target velocity at $t = 0$ (i.e., at time $T_1$). A similar equation holds for the $y$-direction. Since the displacement along the $x$-direction, namely $L_{x2} = x(T_2) - x(0)$, and that along the $y$-direction, namely $L_{y2} = y(T_2) - y(0)$, are proportional to the flight time $T_2$, one obtains:

$$L_{x2} = dx_2 - dx_1 = v_{x1}T_2, \tag{4}$$

$$L_{y2} = dy_2 - dy_1 = v_{y1}T_2. \tag{5}$$

Thus, the velocity at $t = 0$ can be determined as follows:

$$v_{x1} = \frac{dx_2 - dx_1}{T_2}, \tag{6}$$

$$v_{y1} = \frac{dy_2 - dy_1}{T_2}. \tag{7}$$

The equation of motion for the $z$-direction is as follows:

$$m\frac{dv_z}{dt} = -mg, \tag{8}$$

where $g$ is the gravitational acceleration. The $z$-component of the velocity and the position of the target are:

$$v_z(t) = -gt + v_{z1}, \tag{9}$$

$$z(t) = -\frac{g}{2}t^2 + v_{z1}t + (H_1 + dz_1), \tag{10}$$

where $v_{z1}$ is the $z$-component of the target velocity at $t = 0$. The displacement along the $z$-direction, namely $L_{z2} = z(T_2) - z(0)$ is as follows:

$$L_{z2} = (H_2 + dz_2) - (H_1 + dz_1) = -\frac{g}{2}T_2^2 + v_{z1}T_2. \tag{11}$$

The $z$-component of the velocity at $t = 0$ ($v_{z1}$) is as follows:

$$v_{z1} = (L_{z2} + \frac{g}{2}T_2^2)\frac{1}{T_2}. \tag{12}$$

In the absence of an electric field, the target position at time $T_3$ is given by:

$$x''(T_3) = dx_3'' = dx_1 + v_{x1}T_3, \tag{13}$$
$$y(T_3) = dy_3 = dy_1 + v_{y1}T_3, \tag{14}$$
$$z(T_3) = H_3 + dz_3 = -\frac{g}{2}T_3^2 + v_{z1}T_3 + (H_1 + dz_1). \tag{15}$$

The $x$-coordinate of the red point P"$_3$ is obtained using Eq. (13). In reality, an electric field with magnitude $E_0$ exists between the first pair of deflection plates (A).

The equation of motion, velocity, and position of the charged target in the constant electric field $E_0$ for the $x$-direction are:

$$m\frac{dv_x}{dt} = qE_0, \tag{16}$$
$$v_x(t) = \frac{q}{m}E_0t + C_1, \tag{17}$$
$$x(t) = \frac{q}{2m}E_0t^2 + C_1t + C_2, \tag{18}$$

where $q$ is the charge of the target. The integration constants $C_1$ and $C_2$ are determined from the initial conditions. The position depends on the mass-to-charge ratio.

The times $T_{\mathrm{Ain}}$ and $T_{\mathrm{Aout}}$, at which the target enters and exits the region with constant electric field, respectively, are obtained according to:

$$z(T_{\mathrm{Ain}}) = -\frac{g}{2}T_{\mathrm{Ain}}^2 + v_{z1}T_{\mathrm{Ain}} + (H_1 + dz_1) = H_{\mathrm{AU}}, \tag{19}$$

$$z(T_{\mathrm{Aout}}) = -\frac{g}{2}T_{\mathrm{Aout}}^2 + v_{z1}T_{\mathrm{Aout}} + (H_1 + dz_1) = H_{\mathrm{AL}}, \tag{20}$$

where $H_{\mathrm{AU}}$ and $H_{\mathrm{AL}}$ are the upper and lower heights of the A electrodes from the $XY$-plane ($z = 0$). The duration of the constant acceleration of the target is represented by:

$$\Delta T_{\mathrm{A}} = T_{\mathrm{Aout}} - T_{\mathrm{Ain}}. \tag{21}$$

After the target exits the acceleration region, it moves again with constant velocity till $t = T_3$. The positions of the target at times $T_1$, $T_{\mathrm{Ain}}$, $T_{\mathrm{Aout}}$, and $T_3$ are given by:

$$x(T_1) = x(0) = dx_1, \tag{22}$$
$$x(T_{\mathrm{Ain}}) = dx_1 + v_{x1}T_{\mathrm{Ain}}, \tag{23}$$
$$x(T_{\mathrm{Aout}}) = dx_1 + v_{x1}T_{\mathrm{Ain}} + v_{x1}\Delta T_{\mathrm{A}} + \frac{q}{2m}E_0\Delta T_{\mathrm{A}}^2 = dx_1 + v_{x1}T_{\mathrm{Aout}} + \frac{q}{2m}E_0\Delta T_{\mathrm{A}}^2, \tag{24}$$
$$x(T_3) = dx_1 + v_{x1}T_{\mathrm{Aout}} + \frac{q}{2m}E_0\Delta T_A^2 + \left(v_{x1} + \frac{q}{m}E_0\Delta T_{\mathrm{A}}\right)(T_3 - T_{\mathrm{Aout}}) = dx_1 + v_{x1}T_3 + \frac{q}{m}\left[\frac{\Delta T_{\mathrm{A}}^2}{2} + \Delta T_{\mathrm{A}}(T_3 - T_{\mathrm{Aout}})\right]E_0 = dx_3. \tag{25}$$

The $x$-coordinate of the black point $P_3$ is represented using Eq. (25). The $x$-components of the position and velocity at times $T_1$, $T_{\mathrm{Ain}}$, $T_{\mathrm{Aout}}$, and $T_3$ are summarized in Table 2.

Table 2 Position and velocity of the target in the $x$-direction from time $T_1 = 0$ to time $T_3$.

| Time | Position | Velocity |
|---|---|---|
| 0 | $x(0) = dx_1$ | $v_{x1}$ |
| $T_{\mathrm{Ain}}$ | $dx_1$+$v_{x1}T_{\mathrm{Ain}}$ | $v_{x1}$ |
| $T_{\mathrm{Aout}}$ | $dx_1$+$v_{x1}T_{\mathrm{Ain}}$ +$v_{x1}\Delta T_{\mathrm{A}}$+$qE_0\Delta T_{\mathrm{A}}^2/(2m)$ | $v_{x1}$+$(q/m)E_0\Delta T_{\mathrm{A}}$ |
| $T_3$ | $x(T_3) = dx_1$+$v_{x1}T_{\mathrm{Aout}}$ +$qE_0\Delta T_{\mathrm{A}}^2/(2m)$ + $[v_{x1}$+$(q/m)E_0\Delta T_{\mathrm{A}}](T_3 - T_{\mathrm{Aout}})$ | $v_{x1}$+$(q/m)E_0\Delta T_{\mathrm{A}}$ |

The difference between $x(T_3)$ and $x"(T_3)$ is as follows:

$$x(T_3) - x''(T_3) = dx_3 - dx_3'' = \frac{q}{m}\left[\frac{\Delta T_{\mathrm{A}}^2}{2} + \Delta T_{\mathrm{A}}(T_3 - T_{\mathrm{Aout}})\right]E_0. \tag{26}$$

This difference is proportional to the electric field $E_0$. To observe this difference, a sufficiently strong electric field $E_0$ must be applied. The measurement value $dx_3 = x(T_3)$ is obtained experimentally from the $\mathrm{PMU}_3$. The theoretical value $dx"_3 = x"(T_3)$ is calculated from the $\mathrm{PMU}_1$ and $\mathrm{PMU}_2$ data. The mass-to-charge ratio $R$ can be obtained from Eq. (26) according to:

$$R = \frac{m}{q} = \frac{\left[\frac{\Delta T_{\mathrm{A}}^2}{2} + \Delta T_{\mathrm{A}}(T_3 - T_{\mathrm{Aout}})\right]E_0}{dx_3 - dx_3''}. \tag{27}$$

The mass-to-charge ratio of the charged target in flight can then be determined from the $\mathrm{PMU}_1$, $\mathrm{PMU}_2$, and $\mathrm{PMU}_3$ data.

# 4. Control Electric Field

In this section, the control electric field is determined. At time $T_3$, the target has the initial global position ($dx_3$, $dy_3$, $H_3 + dz_3$) and the initial velocity ($v_{x3}$, $v_{y3}$, $v_{z3}$). These values are used to determine the control electric fields $E_x$ and $E_y$. This position and velocity are related to the PMU$_i$ (i = 1, 2, 3) data and the mass-to-charge ratio.

$$x(T_3) = dx_3 = dx_1 + v_{x1}T_{\mathrm{Aout}} + \frac{q}{2m}E_0\Delta T_{\mathrm{A}}^2 + \left[v_{x1} + \frac{q}{m}E_0\Delta T_{\mathrm{A}}\right](T_3 - T_{\mathrm{Aout}}), \tag{25}$$

$$y(T_3) = dy_3 = dy_1 + v_{y1}T_3, \tag{14}$$

$$z(T_3) = H_3 + dz_3 = -\frac{g}{2}T_3^2 + v_{z1}T_3 + (H_1 + dz_1), \tag{15}$$

$$v_x(T_3) = v_{x3} = v_{x1} + \frac{q}{m}E_0\Delta T_{\mathrm{A}}, \tag{28}$$

$$v_y(T_3) = v_{y3} = v_{y1}, \tag{29}$$

$$v_z(T_3) = v_{z3} = v_{z1} - gT_3. \tag{30}$$

The target arrival time $T_4$, which corresponds the time at which target passes through the reactor center in the $XY$-plane (z = 0), is obtained according to:

$$z(T_4) = -\frac{g}{2}T_4^2 + v_{z1}T_4 + (H_1 + dz_1) = 0. \tag{31}$$

Times $T_{\mathrm{Bin}}$ and $T_{\mathrm{Bout}}$ are obtained according to:

$$z(T_{\mathrm{Bin}}) = -\frac{g}{2}T_{\mathrm{Bin}}^2 + v_{z1}T_{\mathrm{Bin}} + (H_1 + dz_1) = H_{\mathrm{BU}}, \tag{32}$$

$$z(T_{\mathrm{Bout}}) = -\frac{g}{2}T_{\mathrm{Bout}}^2 + v_{z1}T_{\mathrm{Bout}} + (H_1 + dz_1) = H_{\mathrm{BL}}, \tag{33}$$

where $H_{\mathrm{BU}}$ and $H_{\mathrm{BL}}$ are the upper and lower heights of the B electrodes, respectively. The duration of the constant acceleration in the $x$-direction is as follows:

$$\Delta T_{\mathrm{B}} = T_{\mathrm{Bout}} - T_{\mathrm{Bin}}. \tag{34}$$

The positions of the target at times $T_3$, $T_{\mathrm{Bin}}$, and $T_{\mathrm{Bout}}$ are

$$x(T_3) = dx_3, \tag{35}$$

$$x(T_{\mathrm{Bin}}) = dx_3 + v_{x3}(T_{\mathrm{Bin}} - T_3), \tag{36}$$

$$x(T_{\mathrm{Bout}}) = dx_3 + v_{x3}(T_{\mathrm{Bin}} - T_3) + v_{x3}\Delta T_{\mathrm{B}} + \frac{q}{2m}E_x\Delta T_{\mathrm{B}}^2 = dx_3 + v_{x3}(T_{\mathrm{Bout}} - T_3) + \frac{q}{2m}E_x\Delta T_{\mathrm{B}}^2. \tag{37}$$

To calculate the control electric field $E_x$, $x(T_4)$ is set to zero. Thus, one obtains:

$$\begin{aligned} x(T_4) &= dx_3 + v_{x3}(T_{\mathrm{Bout}} - T_3) + \frac{q}{2m}E_x\Delta T_{\mathrm{B}}^2 \\ &\quad + (v_{x3} + \frac{q}{m}E_x\Delta T_{\mathrm{B}})(T_4 - T_{\mathrm{Bout}}) \\ &= dx_3 + v_{x3}(T_4 - T_3) + \frac{q}{2m}E_x\Delta T_{\mathrm{B}}^2 \\ &\quad + \frac{q}{m}E_x\Delta T_B(T_4 - T_{\mathrm{Bout}}) \\ &= dx_3 + v_{x3}(T_4 - T_3) \\ &\quad + \frac{q}{m}\left[\frac{\Delta T_{\mathrm{B}}^2}{2} + \Delta T_{\mathrm{B}}(T_4 - T_{\mathrm{Bout}})\right]E_x \\ &= dx_3 + v_{x3}(T_4 - T_3) \\ &\quad + \frac{1}{R}\left[\frac{\Delta T_{\mathrm{B}}^2}{2} + \Delta T_{\mathrm{B}}(T_4 - T_{\mathrm{Bout}})\right]E_x \\ &= 0. \end{aligned} \tag{38}$$

The $x$-components of the position and velocity at times $T_3$, $T_{\mathrm{Bin}}$, $T_{\mathrm{Bout}}$, and $T_4$ are summarized in Table 3.

The electric field $E_x$ is obtained from Eq. (38) as follows:

$$\begin{aligned} E_x &= \frac{-dx_3 - v_{x3}(T_4 - T_3)}{\left[\frac{\Delta T_{\mathrm{B}}^2}{2} + \Delta T_{\mathrm{B}}(T_4 - T_{\mathrm{Bout}})\right]} \cdot R \\ &= \frac{-dx_3 - v_{x3}(T_4 - T_3)}{dx_3 - dx''_3} \cdot \frac{\left[\frac{\Delta T_{\mathrm{A}}^2}{2} + \Delta T_{\mathrm{A}}(T_3 - T_{\mathrm{Aout}})\right]}{\left[\frac{\Delta T_{\mathrm{B}}^2}{2} + \Delta T_{\mathrm{B}}(T_4 - T_{\mathrm{Bout}})\right]} \cdot E_0 \\ &= \frac{-dx_3 - (v_{x1} + \frac{q}{m}E_0\Delta T_{\mathrm{A}})(T_4 - T_3)}{dx_3 - dx''_3} \cdot \frac{\left[\frac{\Delta T_{\mathrm{A}}^2}{2} + \Delta T_{\mathrm{A}}(T_3 - T_{\mathrm{Aout}})\right]}{\left[\frac{\Delta T_{\mathrm{B}}^2}{2} + \Delta T_{\mathrm{B}}(T_4 - T_{\mathrm{Bout}})\right]} \cdot E_0. \end{aligned} \tag{39}$$

A similar analysis holds for the $y$-direction. The $y$-components of the position and velocity of the target are summarized in Table 4.

In the $y$-direction, times $T_{\mathrm{Cin}}$ and $T_{\mathrm{Cout}}$ are obtained according to:

Table 3 Position and velocity of the target in the $x$-direction from time $T_3$ to time $T_4$.

| Time | Position | Velocity |
|---|---|---|
| $T_3$ | $x(T_3) = dx_3$ | $v_{x3} = v_{x1}+(q/m)E_0\Delta T_{\mathrm{A}}$ |
| $T_{\mathrm{Bin}}$ | $dx_3+v_{x3}(T_{\mathrm{Bin}} -T_3)$ | $v_{x3}$ |
| $T_{\mathrm{Bout}}$ | $dx_3+v_{x3}(T_{\mathrm{Bin}} -T_3)$ + $v_{x3}\Delta T_{\mathrm{B}}+qE_x\Delta T_{\mathrm{B}}^2/(2m)$ | $v_{x3}+(q/m)E_x\Delta T_{\mathrm{B}}$ |
| $T_4$ | $x(T_4) = dx_3+v_{x3}(T_{\mathrm{Bout}} -T_3)$ + $qE_x\Delta T_{\mathrm{B}}^2/(2m)$ +$[v_{x3}+(q/m)E_x\Delta T_{\mathrm{B}}](T_4 -T_{\mathrm{Bout}})$ | $v_{x3}+(q/m)E_x\Delta T_{\mathrm{B}}$ |

Table 4 Position and velocity of the target in the $y$-direction from time $T_3$ to time $T_4$.

| Time | Position | Velocity |
|---|---|---|
| $T_3$ | $y(T_3) = dy_3$ | $v_{y3} = v_{y1}$ |
| $T_{\mathrm{Cin}}$ | $dy_3+v_{y3}(T_{\mathrm{Cin}}-T_3)$ | $v_{y3}$ |
| $T_{\mathrm{Cout}}$ | $dy_3+v_{y3}(T_{\mathrm{Cin}}-T_3)$ $+v_{y3}\Delta T_{\mathrm{C}}+qE_y\Delta T_{\mathrm{C}}^2/(2m)$ | $v_{y3}+(q/m)E_y\Delta T_{\mathrm{C}}$ |
| $T_4$ | $y(T_4) = dy_3+v_{y3}(T_{\mathrm{Cout}}-T_3)$ $+qE_y\Delta T_{\mathrm{C}}^2/(2m)$ $+[v_{y3}+(q/m)E_y\Delta T_{\mathrm{C}}](T_4-T_{\mathrm{Cout}})$ | $v_{y3}+(q/m)E_y\Delta T_{\mathrm{C}}$ |

Table 5 Time sequence of the target injection at $v_{z1} = -3$ m/s.

| Time [s] | | Height [m] | $X$ [μm] | $Y$ [μm] |
|---|---|---|---|---|
| 0 | $T_1$ at $\mathrm{PMU_1}$ | 2.0 | 0 | 0 |
| 0.1 | $T_2$ at $\mathrm{PMU_2}$ | 1.651 | 0 | 1000 |
| 0.125 | $T_{\mathrm{Ain}}$ at $H_{\mathrm{AU}}$ | 1.5484 | 0 | 1250 |
| 0.175 | $T_{\mathrm{Aout}}$ at $H_{\mathrm{AL}}$ | 1.3249 | 338 | 1750 |
| 0.2 | $T_3$ at $\mathrm{PMU_3}$ | 1.204 | 675 | 2000 |
| 0.225 | $T_{\mathrm{Bin}}$ at $H_{\mathrm{BU}}$ | 1.0769 | 1013 | 2250 |
| 0.275 | $T_{\mathrm{Bout}}$ at $H_{\mathrm{BL}}$ | 0.8044 | 1128 | 2750 |
| 0.3 | $T_{\mathrm{Cin}}$ at $H_{\mathrm{CU}}$ | 0.659 | 907 | 3000 |
| 0.35 | $T_{\mathrm{Cout}}$ at $H_{\mathrm{CL}}$ | 0.3498 | 464 | 2199 |
| 0.4023084 | $T_4$ | 0.0 | 0 | 0 |

$$z(T_{\mathrm{Cin}}) = -\frac{g}{2}T_{\mathrm{Cin}}^2 + v_{z1}T_{\mathrm{Cin}} + (H_1 + dz_1) = H_{\mathrm{CU}}, \tag{40}$$

$$z(T_{\mathrm{Cout}}) = -\frac{g}{2}T_{\mathrm{Cout}}^2 + v_{z1}T_{\mathrm{Cout}} + (H_1 + dz_1) = H_{\mathrm{CL}}, \tag{41}$$

where $H_{\mathrm{CU}}$ and $H_{\mathrm{CL}}$ are the upper and lower heights of the C electrodes, respectively. The duration of the constant acceleration in the $y$-direction is as follows:

$$\Delta T_{\mathrm{C}} = T_{\mathrm{Cout}} - T_{\mathrm{Cin}}. \tag{42}$$

Thus, using a similar argument, one obtains:

$$E_y = \frac{-dy_3 - v_{y3}(T_4 - T_3)}{\left[\frac{\Delta T_{\mathrm{C}}^2}{2} + \Delta T_{\mathrm{C}}(T_4 - T_{\mathrm{Cout}})\right]} \cdot R. \tag{43}$$

The control electric fields $E_x$ and $E_y$ for the charged target in flight are determined from the $\mathrm{PMU_1}$, $\mathrm{PMU_2}$, and $\mathrm{PMU_3}$ data. The voltage $V$ between the plates can be obtained by multiplying the electric field $E$ by the separation distance $d$ between the plates, i.e., $V = Ed$. In order to generate the potential difference between the plates, the DC power supply does not require a large current but only a high-speed switching response and an accurate voltage control, as shown in Sec. 5.

# 5. Numerical Examples

Two numerical examples are provided as model applications of the proposed trajectory control system. In this section, the gravitational acceleration $g$ and permittivity $\varepsilon_0$ are assumed to be $9.8\,\mathrm{m/s^2}$ and $8.854 \times 10^{-12}$ F/m, respectively.

## 5.1 Design parameters for a tabletop plasma device

The development of a repetitive target injection, tracking, and laser engagement system is crucial for the realization of laser fusion power plants. Experimental repeatability enhances the reliability of a system. A repetitive target shot is also important to acquire reliable plasma atomic data. Many different types of atoms are used in the laser fusion target, which is illuminated by lasers with numerous shot parameters. The proposed trajectory control system can be applied both to the repetitive neutron generation experiment and to the future repetitive plasma generation experiment.

Previous demonstration experiments of the target injection, laser engagement, and neutron generation at 1 Hz were conducted using a HAMA laser [9, 11, 12]. In these works, the authors did not use an electric field trajectory control system but rather a freely falling target and considered a 0.2-m vertical flight path. Considering a typical laboratory room, a vertical flight path of 2 m was selected in the present work. Three pairs of plates, namely the test plates A, control plates B, and control plates C, were set along the path. Furthermore, the $\mathrm{PMU_1}$ and $\mathrm{PMU_2}$ were set at a sufficient distance between each other for target trajectory determination. There should also be a sufficiently large distance between the last pair of plates and the fixed focus of the implosion laser, i.e., the origin of the global coordinate system. The values of the heights of the PMUs and the plates are listed in Table 5. The accuracy of the measurement of the target position was assumed to be 1 μm [8]. The values of the mass $m$, charge $q$, and injection speed $v_{z1}$ of the injected target were chosen based on two factors: (i) easiness of the measurement of the trajectory deflection over 500 μm and (ii) simplicity of the trajectory control. Since our model can measure the trajectory deflection with an accuracy of 1 μm, the relative error in the mass-to-charge ratio $R$ is smaller than 0.004 (= 2/500) according to Eq. (27). As the trajectory deflection is proportional to the electric field $E_0$, then the relative error decreases with increasing $E_0$.

An Fe (density of $7.87\,\mathrm{g/cm^3}$) solid target with a radius $r = 0.5$ mm was chosen. The mass of the target was 4.1207 mg, which is on the same order of the high-gain laser fusion target mass (4.6553 mg) [7]. In addition, steel ball bearings of the same size were used for the trajectory control system. Mori *et al.* pushed the spherical shell target with a needle and obtained an initial velocity of 0.19 m/s [10]. If the needle is charged at 1 kV, the surface voltage of the target $V_0$ also becomes 1 kV. The charge of the target is obtained according to:

$$\frac{q}{4\pi\varepsilon_0 r} = 1000. \tag{44}$$

Thus, the target charge is as follows:

$$q = 4\pi\varepsilon_0 r \times V_0 = 5.5631 \times 10^{-11}. \tag{45}$$

The mass-to-charge ratio $m/q$ is $7.4072 \times 10^4$ kg/C. Although this is an idealized value, the mass-to-charge ratio for each injection is distributed around this value. The electric field between the A test plates is set to be $E_0 = 2 \times 10^4$ V/m. The target position at $t = 0$ is assumed to be $(0, 0, 2)$. As the target is composed of solid Fe, it is not destroyed by the needle impact. The target velocity is assumed to be $(0, 0.01, -3)$ for the high-repetition experiment. The other parameters and time sequence are listed in Table 5.

In reality, the position of the target can be determined with an accuracy of 1 μm, but the height of the deflection plates has an error $\Delta L$ (~0.1 mm) due to machining and installation. As this error results in errors in $T_{\mathrm{Ain}}$, $T_{\mathrm{Aout}}$, $\Delta T_{\mathrm{A}}$, and so on, also the mass-to-charge ratio $R$ and the control electric fields $E_x$ and $E_y$ have an error. The relative error in the plate length is estimated to be 0.0005 (0.1 mm/200 mm), and $\Delta T_{\mathrm{A}}$ has a relative error of ~0.001. Since the velocity of the target is less than 10 m/s, we assume a time resolution of $10^{-7}$ s at $T_2$ and $T_3$ to predict the position of the target at $T_4$ with an accuracy of 1 μm.

The distance from $\mathrm{PMU}_2$ to $\mathrm{PMU}_1$ ($\mathrm{PMU}_3$) is ~0.35 m (~0.45 m), whereas the distance from the fixed focus of the implosion laser to the bottom of the C plates is ~0.35 m. The interaction between the target and the electric field has a duration of 50 ms for all pairs of plates. The displacement of the target due to the electric field $E_0$ at the $\mathrm{PMU}_3$ is 675 μm. The control electric fields, namely $E_x$ between the B plates and $E_y$ between the C plates, are calculated using Eqs. (39) and (43), respectively. They are $-3.313 \times 10^4$ and $-7.709 \times 10^4$ V/m, respectively. If the allowable position error at time $T_4$ is required to be 20 μm, then the allowable relative errors in $E_x$ and $E_y$ are 0.006 and 0.005, respectively. $E_x$ must be applied within 25 ms ($= T_{\mathrm{Bin}} - T_3$) after the target position is monitored at $T_3$.

If the surface voltage of the target is set to 0.5 ($= 1/2$) kV, the $x$-displacement of the target at $\mathrm{PMU}_3$ is 338 ($= 675/2$) μm. $E_x$ and $E_y$ are $-3.313 \times 10^4$ V/m and $-1.542 \times 10^5$ V/m, respectively. As the target charge is halved, the magnitude of the electric field $E_y$ must double.

The lengths of the A, B, and C plates are ~0.22, ~0.27 and ~0.31 m, respectively. The distance between the B and A (C) plates is ~0.25 m (~0.15 m). As the injection velocity is 3 m/s, an injection of $N$ Hz corresponds to a distance of at least $3/N$ m between the targets. If this distance is larger than the plate length, it then becomes possible to inject the target with $N$ Hz. These considerations indicate that this control system can be operated at 9 Hz.

Since the impulse $J$ on the target is calculated as the integral of the force $F$ over the time interval $t$ during which it acts, the velocity change caused by the $E_y$ control plates is written as follows:

$$\mathrm{d}(v_y) = \frac{1}{m} F_y dt = \left(\frac{q}{m}\right) E_y dt \cong \left(\frac{4\pi\varepsilon_0 r\, V_0}{m}\right) E_y \frac{L}{v_z}, \tag{46}$$

where $L$ is the length of the plate. If the $E_y$ control plates are set at the midpoint of the vertical path and the target has a $y$-component of the initial velocity $v_{y1} \neq 0$, then the change in $v_y$ at the midpoint required for the target to hit the fixed focus of the implosion laser is as follows:

$$\mathrm{d}(v_y) = -2v_{y1} \cong \frac{4\pi\varepsilon_0 r\, V_0 L}{m v_z} E_y. \tag{47}$$

The value of $E_y$ must be smaller than the maximum electric field $E_{y\max}$ that the apparatus can generate. Considering Eq. (47), one obtains:

$$2\Delta v_{y\max} \sim \left| \frac{4\pi\varepsilon_0 r\, V_0 L}{m v_z} E_{y\max} \right|, \tag{48}$$

where $\Delta v_{y\max}$ is the tolerance of the initial $y$-component velocity at the target injection, i.e., $-\Delta v_{y\max} < v_{y1} < \Delta v_{y\max}$. The inequality in Eq. (48) provides a limited range for the design parameters. If we assume $E_{y\max} = 2$ kV/cm, $L = 0.2$ m and $v_z = 5$ m/s, the right-hand side of Eq. (48) then becomes:

$$\left| \frac{5.563132 \times 10^{-11} \times 0.2 \times 2 \times 10^5}{4.1207 \times 10^{-6} \times 5} \right| \approx 0.1, \tag{49}$$

and the value of $\Delta v_{y\max}$ is 0.05 m/s. Since Eq. (48) holds for a simple one-stage control system, a similar inequality holds for a multistage control system, i.e.:

$$2\Delta v_{y\max} \sim \left| \frac{4\pi\varepsilon_0 r\, V_0}{m v_z} \sum\nolimits_{\mathrm{i}} L_{\mathrm{i}} E_{y\mathrm{imax}} \right|, \tag{50}$$

where $L_{\mathrm{i}}$ and $E_{y\mathrm{imax}}$ are the length and the maximum electric field of the $i$-th plates, respectively.

The proposed control system has only three pairs of deflection plates, namely A, B, and C. Auxiliary control plates B' and C' may be set to adjust the trajectory more precisely with additional PMUs.

## 5.2 Design parameters for a laser fusion reactor

As the surface temperature of a laser fusion reactor chamber exceeds 900 K, the injection velocity of the target is greater than 100 m/s to retain the solid hydrogen layer at the implosion shot against the infrared radiation. Considering Eq. (48), when the target velocity $v_z$ is increased to 100 m/s, the charging voltage $V_0$, plate length $L$, and maximum electric field $E_{\max}$ must be increased accordingly to extend the tolerance of the initial velocity components, namely $\Delta v_{x\max}$ and $\Delta v_{y\max}$. The target is in contact with a metal support, to which a voltage of 2 kV is applied. Thus, the surface voltage of the target is assumed to be $V_0 = 2$ kV

at the moment of target injection. The mass and radius of the target are assumed to be 4 mg and 2 mm, respectively. The charge of the target is obtained according to:

$$\frac{q}{4\pi\varepsilon_0 r} = 2000. \tag{51}$$

Thus, the target charge is as follows:

$$q = 4\pi\varepsilon_0 r \times V_0 = 4.4505 \times 10^{-10}. \tag{52}$$

The mass-to-charge ratio $m/q$ is calculated to be $8.9877 \times 10^3$ kg/C. The electric field between the A test plates is set to $E_0 = 1\times10^5$ V/m. The position and velocity of the target at $t = 0$ are assumed to be $(0, 0, 13)$ and $(0.1, 0.1, -100)$, respectively. The other parameters and the time sequence are listed in Table 6. Since the velocity of the target is ~100 m/s, we assume a time resolution of $10^{-8}$ s at $T_2$ and $T_3$ to predict the position of the target at $T_4$ with an accuracy of 1 μm.

The distance from the $PMU_2$ to the $PMU_1$ ($PMU_3$) is 1.5 m (2.0 m), whereas the distance from the reactor center to the bottom of the C plates is 5.5 m. The interaction between the target and the electric field has a duration of ~15 ms for all pairs of plates. The displacements of the target in the $x$- and $y$-directions at the $PMU_3$ are 5154 (= 3494 + 1660) and 3494 μm, respectively. The displacement of the target due to the electric field $E_0$ is 1660 μm. The control electric fields, namely $E_x$ between the B plates and $E_y$ between the C plates, are calculated using Eqs. (39) and (43), respectively. They are $-2.228 \times 10^5$ and $-1.259 \times 10^5$ V/m in the case of $E_0 = 1 \times 10^5$ V/m, respectively. If the allowable position error at time $T_4$ is required to be 20 μm, then the allowable relative errors in $E_x$ and $E_y$ are 0.0006 and 0.0015, respectively.

The direction and strength of the electric field $E_0$ between the A test plates are important for reducing the strength of the electric field $E_x$ between the B test plates. If the electric field between the A test plates is set to $E_0 = -1 \times 10^5$ V/m, the displacement of the target at the $PMU_3$ is 1834 (= 3494 − 1660) μm. The control electric fields $E_x$ and $E_y$ are $-3.262 \times 10^4$ and $-1.259 \times 10^5$ V/m in the case of $E_0 = -1 \times 10^5$ V/m, respectively. If the allowable position error at time $T_4$ is required to be 20 μm, then the allowable relative errors in $E_x$ and $E_y$ are 0.004 and 0.0015, respectively. This result indicates that whether $1\times10^5$ V/m or $-1\times10^5$ V/m can be adequately determined after monitoring the $PMU_1$ and $PMU_2$ so as to decrease the absolute value of $E_x$ for fine control. Moreover, the value of the mass-to-charge ratio is roughly known before the injection; thus, after obtaining the data from the $PMU_1$ and $PMU_2$, the adequate value of $E_0$ for measuring the mass-to-charge ratio can be determined so as to decrease $|E_x|$.

Table 6 Time sequence of the target injection at $v_{z1} = -100$ m/s.

| Time [s] | | Height [m] | $X$ [μm] | $Y$ [μm] |
|---|---|---|---|---|
| 0 | $T_1$ at $PMU_1$ | 13 | 0 | 0 |
| 0.01498899 | $T_2$ at $PMU_2$ | 11.5 | 1499 | 1499 |
| 0.01748502 | $T_{Ain}$ at $H_{AU}$ | 11.25 | 1749 | 1749 |
| 0.03244841 | $T_{Aout}$ at $H_{AL}$ | 9.75 | 4490 | 3245 |
| 0.03494018 | $T_3$ at $PMU_3$ | 9.5 | 5154 | 3494 |
| 0.03992191 | $T_{Bin}$ at $H_{BU}$ | 9 | 6482 | 3992 |
| 0.05485257 | $T_{Bout}$ at $H_{BL}$ | 7.5 | 7698 | 5485 |
| 0.05982463 | $T_{Cin}$ at $H_{CU}$ | 7 | 7183 | 5982 |
| 0.07472638 | $T_{Cout}$ at $H_{CL}$ | 5.5 | 5640 | 5918 |
| 0.12918228 | $T_4$ | 0.0 | 0 | 0 |

The control electric field $E_x$ must be applied within 5 ms (= $T_{Bin} - T_3$) after the target position is monitored at $T_3$. The electric field is created between pairs of deflection plates. We consider the charging time of the deflection plates. We assume that plates have a width $w = 0.02$ m, a length $L = 1.5$ m, and a separation distance $d = 0.02$ m. The parallel plates can be considered to be a capacitor. The capacitance of the deflection plates is $1.328 \times 10^{-11}$ F.

We assume that each plate has an electric wire connected in series with a resistor $R = 10\,\text{k}\Omega$ to reduce the electric current. The RC time constant $\tau$ is the product of the circuit resistance $R$ and the circuit capacitance $C$, i.e., $\tau = 1.328 \times 10^{-7}$ s. One of deflection plates is connected to ground ($V = 0$), whereas the other is assumed to be connected to a high-voltage terminal $V = V_{high}$ at $t = 0$. The potential difference between the plates is $V(t) = V_{high} \times (1 - e^{-t/RC})$. At $t = 9.296 \times 10^{-7}$ s (= $7\tau$), the potential difference becomes $V_{high} \times (1 - 0.9 \times 10^{-4}) = 0.9991 V_{high}$. The charging time of the deflection plates required to generate the control electric field with a relative error of $10^{-3}$ is shorter than 1 μs. This charging time is much shorter than 5 ms (= $T_{Bin} - T_3$).

Improvements to the injection accuracy of the target can also reduce $|E_x|$ and $|E_{y.}|$. Equation (48) indicates that if the tolerance of the initial $y$-component velocity $\Delta v_{y\max}$ decreases, then the required $E_{y\max}$ also decreases.

The region above the shutter ($z > 5$ m) is assumed to be in vacuum. In a typical reactor using liquid metal, the region below the shutter ($z < 5$ m) is a gas environment. The case whereby the target is injected into the reactor chamber filled with a residual gas is considered. This residual gas acts as a frictional force on the target motion and causes a delay in the arrival time of the target. The arrival time of the vertically injected target is calculated according to the z-component of the data of the target position. Since the frictional force on the target is proportional to the target velocity and $|v_{z1}|$ (> 100 m/s) is much greater than $|v_{x1}|$ (< 0.1 m/s) and $|v_{y1}|$ (< 0.1 m/s), the $x$- and $y$-components of the target velocity in the reactor chamber can be assumed to be constant. Norimatsu *et al*. estimated that the delay is $1.26 \times 10^{-2}$ m in a laser fusion reactor, where the target injection velocity is 200 m/s and the flight distance is 5 m in a 0.05-torr Pb vapor environment [15]. The delay time is thus $6.3 \times 10^{-5}$ s. The delay of the target causes an error in the target position in the $XZ$-plane, as shown in Fig. 4 (a). The timing correction represents a simple adjustment method.

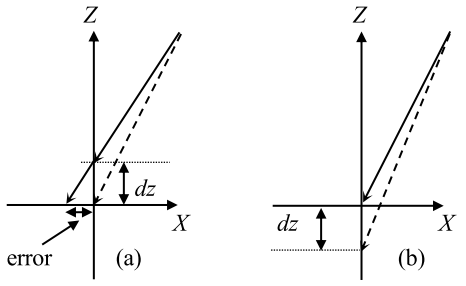


Fig. 4 (a) Before correction. (b) After correction. The solid arrows show the actual trajectory, whereas the dashed arrows show the calculated trajectory without the residual gas effect. $dz$ is the delay of the target caused by the gas resistance.

The timing of the implosion laser shot is adjusted in practice by monitoring the delay of the target in the gas-filled reactor chamber. To monitor the delay of the target, an optical target position measurement is required in the reactor [13, 14]. If the target delay $dz$ can be treated as a constant value in the steady operational reactor, the arrival time $T_4$ will then become $T_4 + (dz/|v_z|)$. If the control electric fields $E_x$ and $E_y$ are calculated using this value, the position error is then eliminated. This procedure means that the injection system aims at $(0, 0, -dz)$, as shown in Fig. 4 (b). If the target position is $(X_0, Y_0, dz)$ at time $T_4$ instead of (0, 0, 0) due to the constant horizontal gas flow, a similar correction (i.e., the injection system aims at $(-X_0, -Y_0, -dz)$) must then be adopted.

Strictly speaking, the target path is divided into two regions: the outside and inside of the reactor, i.e., vacuum and the gas environment. Depending on the region, the target motion must be analyzed using either the equation of motion in vacuum or the equation of motion in the gas environment [13].

As the control electric field $E_x$ is determined by Eq. (39), the target position at $T_4$ is $x(T_4) = 0$. Without the control electric field $E_x$, the $x$-component of the position at time $T_4$ is $x(T_4) = dx_3 + v_{x3}(T_4 - T_3)$. The position displacement required by $E_x$ is $[-dx_3 - v_{x3}(T_4 - T_3)]$. The position displacement is proportional to the value of $E_x$. If $E_x$ becomes $E_x \times (1 + \delta)$, then $x(T_4) = [-dx_3 - v_{x3}(T_4 - T_3)] \times \delta$. This means that the error in the control electric field causes an error in the position of the target at time $T_4$. If the required position displacement is 5000 μm and the allowable position error at time $T_4$ is 20 μm, then $\delta$ must be smaller than 0.004.

Another error may originate from the quantization of the applied voltage in the control system. We consider that the potential difference between the deflection plates is given by the voltage drop of finite resistors. If there are wires and $M$ resistors with resistances $R$, $2R$, $2^2R$ $2^3R, \ldots, 2^{M-1}R$, then we can construct a new resistor $R_A$ with resistance $N \times R$ ($0 < N < 2^M - 1$, where $N$ is an integer) by connecting the wires and several resistors in series. We can construct another new resistor $R_B$ with resistance $(2^M - 1 - N) \times R$ by connecting all the remaining resistors and wires in series.

Here, we add one more resistor with resistance $R$. $M+1$ resistors can be used to construct a new resistor $R_A$ with resistance $N \times R$ ($0 < N < 2^M$, where $N$ is an integer) and a new resistor $R_B$ with resistance $(2^M - N) \times R$. The series resistance of $R_A$ and $R_B$ is $2^M \times R$. We assume that the DC power supply has two terminals, $V = 0$ and $V = V_{max}$. The $R_A$ and $R_B$ resistors are assumed to be connected to both terminals. The electric current is given by $I = V_{max}/(2^M R)$, and the voltage drops of the resistor $R_A$ and $R_B$ are $V_{max} \times (N/2^M)$ and $V_{max} \times (2^M - N)/2^M$, respectively.

The voltage applied between the deflection plates is generated by bringing each deflection plate into contact with both ends of the resistor $R_A$. The quantized voltage interval, i.e., the quantization error in the voltage, is written as $V_{max}/2^M$. Since the maximum position displacement of the target in this control system $dr_{max}$ is proportional to $E_{max}$ and $E_{max}$ is proportional to $V_{max}$ ($= E_{max} d$, where $d$ is the plate separation distance), the quantization error in the voltage $V_{max}/2^M$ then results in a quantization error in the target position $dr_{max}/2^M$. This value must be smaller than 20 μm, which is the allowable position error at time $T_4$:

$$\frac{dr_{max}}{2^M} < 2 \times 10^{-5}. \tag{53}$$

One way to satisfy Eq. (53) is to increase $M$. From Table 6, we consider the case in which the tolerance of the initial $y$-component velocity at the target injection $\Delta v_{ymax}$ is 0.1 m/s. If there is no electric field in this control system, then $y(T_4)$ is 0.013 m, and we obtain $dr_{max} = 0.013$ m. We need at least 11 resistors ($M = 10$) to satisfy Eq. (53). Another way to satisfy Eq. (53) is to decrease $dr_{max}$. If $\Delta v_{ymax}$ is halved, then the quantization error in the target position is also halved.

After the determination of the control electric fields $E_x$ and $E_y$, the potential differences $V_x$ between the B plates and $V_y$ between the C plates are calculated. The values of $V_x$ and $V_y$ are normalized by $V_{max}$ and converted to two binary numbers. Using these binary numbers, resistor selection and circuit construction are realized through switching. The switching time of the relay is a few milliseconds, but the switching time of the FET is usually shorter than 1 μs. The FET switching time is much shorter than 5 ms ($= T_{Bin} - T_3$).

The flight distance of the target from the injection point to the shutter of the reactor is large. A multistage trajectory control system is then considered. The purpose of the first stage is to estimate roughly the $m/q$ value of the target and adjust roughly the target trajectory over a short distance. The purpose of the second stage is to estimate precisely the $m/q$ value and adjust precisely the target trajectory over a long distance. The second stage is easily combined with the first stage. The maximum control electric field of the

second stage $E_{max2}$ can be reduced compared with that of the first stage $E_{max1}$. As indicated by Eq. (53), a reduction in the maximum control electric field leads to a reduction in the quantization error in the control trajectory and to a fine control.

## 6. Conclusion

A method to control the trajectory of a vertically injected charged spherical target was presented. The charged target passes between the test deflection plates. The mass-to-charge ratio of the target was calculated via simple algebraic arithmetic using the local coordinates and time data of the target in the PMU. The magnitude of the applied electric field required to adjust the trajectory of the injected target in order for it to reach the reactor center was calculated using the mass-to-charge ratio as well as the local coordinates and time data of the target. Numerical examples for the control of the injected target in a tabletop high-repetition plasma experimental device and in a laser fusion reactor were provided. A simple criterion for choosing the design parameters of the trajectory control system was obtained.

## Acknowledgments

This work was supported by JSPS KAKENHI Grant Number 20K21015.

## Appendix A. Effect of the Fringe Field of the Parallel Deflection Plate

The electric field is assumed to exist only between the deflection plates. In order to validate this assumption, we introduce a conformal mapping and two coordinate systems, namely the $\omega$-plane and $z$-plane coordinate systems, that have no connection with the $XYZ$-coordinate system. We consider the electric field between two infinite parallel plates set at $v = +\pi(-\pi)$ and charged $\psi = +V(-V)$. In this case, the plates have an infinite width along the direction perpendicular to the $\omega$-plane. Our problem can thus be treated in two dimensions, as shown in Fig. A1 [16–20].

In Fig. A1 (a), the equipotential lines are represented by horizontal solid lines of the form $v = C_1$, and the electric field lines are represented by vertical dashed lines of the form $u = C_2$. As shown in Fig. A1 (b), the electric field between two semi-infinite ($x < -1$) parallel plates can be calculated via conformal mapping in two dimensions [16, 17, 20]:

$$z = x + iy = \omega + \exp(\omega) = u + iv + \exp(u + iv). \tag{A.1}$$

Both positive ($u > 0$, dashed segment) and negative ($u < 0$, solid segment) parts of the $v = +\pi(-\pi)$ line in Fig. A1 (a) are mapped on the segment $y = +\pi(-\pi)$ for $x < -1$ in Fig. A1 (b). This mapping takes the strip ($-\pi < v < \pi$) into the entire $z$-plane. Considering the real and imaginary

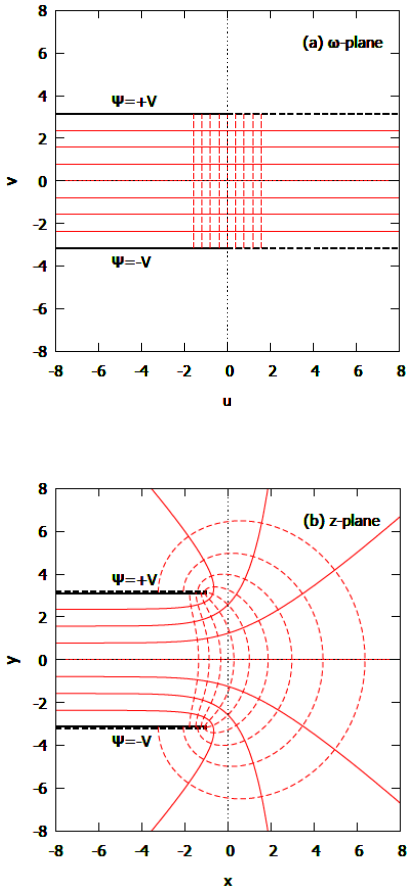


Fig. A1 (a) Two infinite parallel plates and the $\omega$-plane: the horizontal solid line shows an equipotential line at $v = m\pi/4$ ($m = -3 \sim 3$, integer), whereas the vertical dashed line shows the electric field line at $u = n\pi/8$ ($n = -4 \sim 4$, integer). (b) Two semi-infinite parallel plates and the $z$-plane.

parts, it is possible to write:

$$x = u + \exp(u)\cos(v), \tag{A.2}$$

$$y = v + \exp(u)\sin(v). \tag{A.3}$$

The equipotential lines and the electric field lines between two infinite parallel plates in the $\omega$-plane are also mapped into the equipotential lines and the electric field lines between two semi-infinite parallel plates in the $z$-plane, respectively.

The electric field in the $z$-plane is expressed as follows:

$$E_x(x(u,v), y(u,v)) = \frac{V}{\pi} \cdot \frac{e^u \sin v}{1 + 2e^u \cos v + e^{2u}}, \tag{A.4}$$

$$E_y(x(u,v), y(u,v)) = -\frac{V}{\pi} \cdot \frac{1 + e^u \cos v}{1 + 2e^u \cos v + e^{2u}}. \tag{A.5}$$

Examples of coordinate mappings are presented in Table A1.

The fringe field decreases rapidly with the distance from the boundary of the plate. The distance from the

Table A1 $(x(u, v), y(u, v))$ coordinates in the $z$-plane.

| | $u=0$ | 1 | 2 | 8 |
|---|---|---|---|---|
| $v=\pi$ | $(0-e^0, \pi)$ | $(1-e^1, \pi)$ | $(2-e^2, \pi)$ | $(8-e^8, \pi)$ |
| $\pi/2$ | $(0, \pi/2+e^0)$ | $(1, \pi/2+e^1)$ | $(2, \pi/2+e^2)$ | $(8, \pi/2+e^8)$ |
| 0 | $(0+e^0, 0)$ | $(1+e^1, 0)$ | $(2+e^2, 0)$ | $(8+e^8, 0)$ |
| $-\pi/2$ | $(0, -\pi/2-e^0)$ | $(1, -\pi/2-e^1)$ | $(2, -\pi/2-e^2)$ | $(8, -\pi/2-e^8)$ |
| $-\pi$ | $(0-e^0, -\pi)$ | $(1-e^1, -\pi)$ | $(2-e^2, -\pi)$ | $(8-e^8, -\pi)$ |

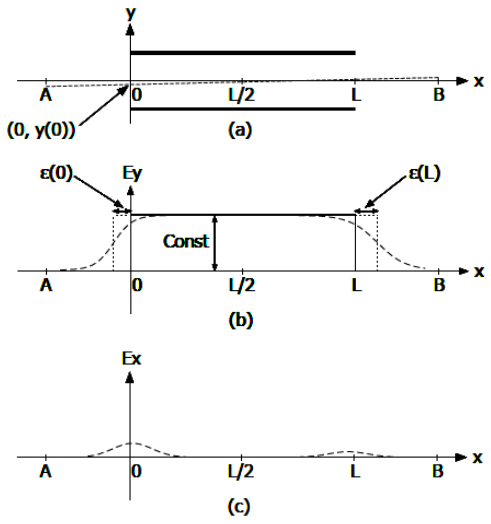


Fig. A2 (a) The dashed line represents the target path between two parallel electrodes placed at $y = \pm\pi$. (b) Electric field $E_y$ as a function of the $x$-component of the target path $(x, y(x))$. The dashed curve represents $E_y$ on the target path. The thick solid line represents a rectangular function. The thin solid line represents an equivalent rectangular function including the effect of the fringe field. (c) Electric field $E_x$ as a function of the $x$-component of the target path.

$(0, 0)$ point to the $(8, 0)$ point in the $\omega$-plane is 1.27 times larger than the spacing between the plates $(2\pi)$. The corresponding distance from the $(1, 0)$ point to the $(8 + e^8, 0)$ point in the $z$-plane is 2987.96, which is 476 times larger than $2\pi$.

We consider the case in which the target is moved through the electrodes of length $L$ and their separation distance $2\pi$ at a constant velocity $(V_{x0}, V_{y0})$, as shown in Fig. A2 (a). The electric field leaks at both boundaries $(x = 0$ and $x = L)$. The electric fields $E_x$ and $E_y$ that the target is subjected to are represented by a solid line in Fig. A2 (c) and a dashed line in Fig. A2 (b) as a function of the $x$-coordinate of the target position, respectively.

Since the impulse $J_y$ is the integral of the force $F_y$, the integral of the smooth function of the dashed curve in Fig. A2 (b) can be approximated by the integral of the thin solid rectangular function to maintain the integral value constant.

$$J_y = \int_{T_A}^{T_B} F_y(t)dt = \int_{T_A}^{T_B} qE_y(x(t), y(x(t)))dt, \tag{A.6}$$

where $F_y$ is the $y$-component of the force that acts on the target, and $T_A$ and $T_B$ are the times at which the target passes $x(T_A) = A$ and $x(T_B) = B$, respectively. Equation (A.6) can be transformed into:

$$\frac{q}{V_{x0}}\int_A^{L/2} E_y(x, y(x))dx + \frac{q}{V_{x0}}\int_{L/2}^{B} E_y(x, y(x))dx = \frac{q}{V_{x0}}\left(-\frac{V}{\pi}\right)\times\left(\left[\varepsilon(0)+\frac{L}{2}\right]+\left[\frac{L}{2}+\varepsilon(L)\right]\right). \tag{A.7}$$

Here, the values $\varepsilon(0)$ and $\varepsilon(L)$ can be considered as the effective length of the plate extension. Assuming the electric field $E_y$ is a constant $-V/\pi$ in the interval $[0, L]$, the value of $\varepsilon(0)$ depends on the $y$-component of the point $(0, y(0))$ and the interval $[A, 0]$.

Since the $x$-coordinate of the plate right edge is $-1$ in Fig. A1 (b), the effective length $\varepsilon(L)$ can be approximated by solving the following equation:

$$\int_{-1}^{-1+D} E_y(x, y(x))dx = -\frac{V}{\pi}\varepsilon, \tag{A.8}$$

where $D$ is the length of the integral interval. The function $y(x)$, i.e., the target path, slowly changes with $x$. We assume that the target passes through the central region $|y(x)| < \pi/2$. The integral is characterized by the position of the target at $y(-1)$ and the integral interval. From Eq. (A.5), one can then obtain:

$$\varepsilon = \int_{-1}^{-1+D} \frac{1 + e^{u(x,y(x))}\cos v(x, y(x))}{1+2e^{u(x,y(x))}\cos v(x, y(x))+e^{2u(x,y(x))}}dx. \tag{A.9}$$

If we consider the effective length of the plate extension, times $T_{\mathrm{Ain}}$ and $T_{\mathrm{Aout}}$ must be calculated according to Eqs. (19) and (20) using the corrected height of the plate, i.e., corrected $H''_{\mathrm{AU}}$ and $H''_{\mathrm{AL}}$.

We consider the case in which the target is moved from the boundary $x = -1$, i.e., from the point S to the point R shown in Fig. A3 (a). The integral of field $(E_x, iE_y)$ along the closed PQRSP path in the $z$-plane is zero according to the Cauchy integral theorem. The integral of the field $(0, -iV/\pi)$ along the corresponding P'Q'R'S'P' path in the $\omega$-plane is also zero.

Since the target motion is bounded near the $x$-axis, the potential difference between the points Q and R can be neglected in the case of a long flight path. This means that the integral along the QR and Q'R' paths can be neglected in the case of a long flight path. In this case, the integral along the SR(S'R') path is the sum of the integral along the SP(S'P') path and the integral along PQ(P'Q') path. The integral along the SP(S'P') path represents mainly the

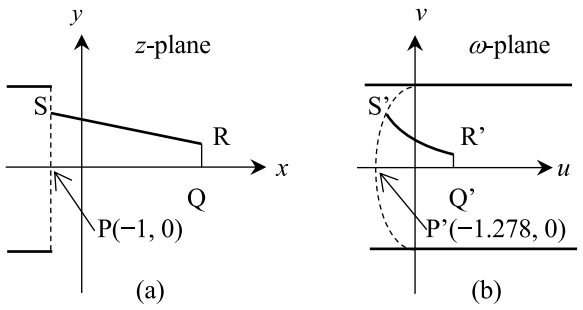


Fig. A3 (a) The segment SR is the target path in the $z$-plane. The points P and Q are the projections of the points S and R, respectively. The thick solid line represents the electrode $y = \pm\pi$ ($x < -1$). (b) The curve S'R' is the corresponding target path in the $\omega$-plane. The points P', Q', R', and S' correspond to the points P, Q, R, and S, respectively. The thick solid line represents the electrode $y = \pm\pi$.

potential energy difference and slows or accelerates the target motion, which depends on the $y$-component of the point S(S'). We can approximate the integral along the SR(S'R') path with the integral along the PQ(P'Q') path.

Considering that the target moves on the $x$-axis ($y = 0$) with a flight distance $D = 2989$ from the right boundary ($x = -1$), then $v = 0$, and the effective length can be bounded as

$$\begin{aligned}\varepsilon &\sim \int_{-1}^{-1+D} \frac{1 + e^{u(x,0)} \cos v(x,0)}{1 + 2e^{u(x,0)} \cos v(x,0) + e^{2u(x,0)}} dx \\ &= \int_{-1}^{2988} \frac{1 + e^{u(x)}}{1 + 2e^{u(x)} + e^{2u(x)}} dx \\ &= \int_{-1.278}^{8} \frac{1 + e^{u}}{1 + 2e^{u} + e^{2u}} \cdot \frac{dx}{du} du \\ &= \int_{-1.278}^{8} dx < 3\pi. \end{aligned} \tag{A.10}$$

The effective length $\varepsilon$ is not more than 1.5 times the plate separation distance $d$.

In practice, as the plate width $w$ is finite and assumed to be $w = d = 0.02$ m, the electric field from the edge of the plate diverges in three dimensions and thus decreases more rapidly. If the deflection plates are set in an electrostatic shield with holes, the electric field can be confined within the shield, as shown in Fig. A4. This results in a decrease in the integral interval $D$ along the $x$-direction and a decrease in the effective length $\varepsilon$.

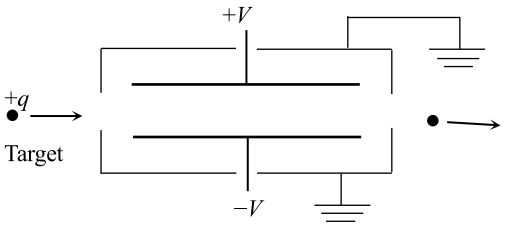


Fig. A4 Electrodes in the electrostatic shield with holes.

The meaning of the effective length $\varepsilon$ is that the length of the control plate $L$ can be considered to be effectively $L+\varepsilon$. As the value of the effective length $\varepsilon$ is on the order of the plate separation distance $d$, the duration of the constant acceleration, i.e., $\Delta T_A$, $\Delta T_B$, and $\Delta T_C$, has a relative error in $d/L$. These errors cause an error in the position of the target at the reactor center. This position error will be compensated in two ways: (1) by installing auxiliary control plates B' and C' to adjust the trajectory more precisely with additional PMUs and (2) using an experimentally obtained correction factor for the control electric field.

[1] D. Goodin *et al*., Fusion Eng. Des. **60**, 27 (2002).
[2] R. Tsuji, Fusion Eng. Des. **81**, 2877 (2006).
[3] T. Kassai and R. Tsuji, J. Phys. Conf. Ser. **112**, 032047 (2008).
[4] R. Petzoldt *et al*., Fusion Sci. Technol. **52**, 459 (2007).
[5] R. Petzoldt *et al*., Fusion Sci. Technol. **56**, 417 (2009).
[6] M. Horowitz *et al.*, Phys. Rev. **88**, 1182 (1952).
[7] S. Bodner *et al*., Fusion Eng. Des. **60**, 93 (2002).
[8] K. Saruta and R. Tsuji, Jpn. J. Appl. Phys. **47**, 1742 (2008).
[9] Y. Mori *et al*., Fusion Sci. Technol. **75**, 36 (2019).
[10] Y. Mori *et al*., Nucl. Fusion **59**, 096022 (2019).
[11] O. Komeda *et al*., Plasma Fusion Res. **8**, 1205020 (2013).
[12] O. Komeda *et al*., Sci. Rep. **3**, 2561 (2013).
[13] R. Tsuji, Plasma Fusion Res. **14**, 3405164 (2019).
[14] R. Tsuji *et al*., J. Phys. Conf. Ser. **688**, 012124 (2016).
[15] T. Norimatsu *et al*., Fusion Sci. Technol. **43**, 339 (2003).
[16] J. Brown and R. Churchill, *Complex Variables and Applications* 8 th ed. (McGraw-Hill, New York 2009) p. 401.
[17] H. Kober, *Dictionary of Conformal Representation* (Dover Publications, New York 1957) p. 116.
[18] K. Binns and P. Lawrenson, *Analysis and Computation of Electric and Magnetic Field Problems* 2 nd ed. (Pergamon Press, Oxford 1973) p. 156.
[19] J. Jeans, *The Mathematical Theory of Electricity and Magnetism* 5 th ed. (Cambridge University Press, London 1925) p. 274.
[20] H. Lamb, *Hydrodynamics* 6 th ed. (Cambridge University Press, London 1932) p. 74.